Liquefaction assessment by SDMT and CPTU in Puerto Baquerizo after Mw6.6 Balao earthquake (Ecuador)

Author1

Christian Ramirez, Eng.

ESPOL Polytechnic University, Escuela Superior Politécnica del Litoral, ESPOL, Department of Earth Sciences, Campus Gustavo Galindo Km 30.5 Vía Perimetral, P.O Box 09-01-5863, Guayaquil, Ecuador.

Author2

Davide Besenzon, MSc.

ESPOL Polytechnic University, Escuela Superior Politécnica del Litoral, ESPOL, Department of Earth Sciences, Campus Gustavo Galindo Km 30.5 Vía Perimetral, P.O Box 09-01-5863, Guayaquil, Ecuador.

Author3

Maurizio Mulas, PhD.

ESPOL Polytechnic University, Escuela Superior Politécnica del Litoral, ESPOL, Department of Earth Sciences, Campus Gustavo Galindo Km 30.5 Vía Perimetral, P.O Box 09-01-5863, Guayaquil, Ecuador.

Author4

Sara Amoroso, PhD.

University of Chieti-Pescara, Department of Engineering and Geology, Pescara, Italy,
Istituto Nazionale di Geofisica e Vulcanologia, L'Aquila, Italy.

Author5

Kerwin Chunga, MSc.

Universidad Técnica de Manabí, Departamento de Construcciones civiles, Portoviejo, Ecuador.

Corresponding author: Davide Besenzon**,** Escuela Superior Politécnica del Litoral, ESPOL, Department of Earth Sciences, Campus Gustavo Galindo Km 30.5 Vía Perimetral, P.O Box 09-01-5863, Guayaquil, Ecuador, besenzon@espol.edu.ec

Abstract

On March 2023, a Mw6.6 intraplate earthquake with epicenter in the Gulf of Guayaquil impacted the coastal region of Ecuador, causing at least 13 deaths, 89 destroyed buildings and 192 affected structures. In several locations around the epicenter of the event, expressions of liquefaction were documented. In order to assess the applicability of liquefaction potential evaluation models, one seismic dilatometer test (SDMT) and one cone penetration test (CPTu) were performed in Puerto Baquerizo (South coastal region of Ecuador, 35 km far from the epicenter), where evidence of earthquake-induced soil liquefaction was clearly observed. In addition, morphological and componentry characterization were carried out in samples of the ejected material retrieved during the exploration program. The liquefaction assessment results in terms of safety factors and liquefaction potential indices reveal that the probability of liquefaction triggering is adequately predicted at the study site by the methodologies based on the SDMT and CPTu data.

Keywords: soil liquefaction, seismic dilatometer test, cone penetration test, 2023 Balao earthquake

1. Introduction

In recent decades great efforts have been dedicated to the development of methodologies that allow reliable prediction of the liquefaction potential, as well as strategies to mitigate its effects in engineering projects. The most widespread procedures in practice are those that are based on field test results. These methods focus on approximating the cyclic resistance of the material using empirical correlations with field test results, and on comparing them with the shear stress levels that are expected to be induced by a specific seismic event [1-3].

The applicability of these procedures is constantly evaluated, by determining whether the occurrence and/or severity of liquefaction predicted by the different models coincides with the liquefaction expressions observed in new case studies. However, although Ecuador is a highly seismic country, there are few cases where earthquake-induced soil liquefaction has been well-documented with observations and field tests. The 2016 Mw7.8 Pedernales earthquake, an interplate subduction earthquake occurred off the coast of Manabi, Ecuador, being the primary source of case histories [4-9] .

This paper aims to compare the predicted levels of liquefaction severity in Puerto Baquerizo City, near Balao, using piezocone test (CPTu) and seismic dilatometer test (SDMT) results with the actual ground damage observed after the 2023 Mw 6.6 earthquake. The earthquake occurred at a depth of 66.4 kilometers, approximately 10 kilometers from Balao in the province of Guayas. Additionally, the grain size and morphological analysis of two samples of ejected recovered sand are also presented for the case study.

2. Geological Setting of Puerto Baquerizo

In the inner estuary of the Gulf of Guayaquil, lithological units of Cretaceous, Tertiary ages emerge, and are mostly covered by Quaternary sediments, of alluvial, alluvial-estuarine, and alluvial-colluvial types [10].

The bedrock belongs to the Pallatanga geological formation, predominantly consisting of Cretaceous basalt, which generates hornfels upon contact with the Chaucha batholith [11]. Upper Cretaceous (Senonian-Maastrichtian) volcano-sedimentary rocks have minor outcrops on some islets in the inner estuary of Guayaquil. On Puná Island, other lithological sedimentary units from geological formations (Miocene-Pliocene age) such as Cerro Mala, Placer, Lechuza, and Puná are delineated [12].

The marine sedimentary sequences, belonging to the Angamarca Group of the Paleogene, are in unconformity over the oceanic basement. These sequences include turbiditic sediments with ash intercalations [11]. Recent alluvial deposits, alluvial-estuarine and alluvial-colluvial, are composed of clays, sands, and gravels, containing a large amount of eroded materials transported from the northern Andes. These deposits form alluvial fans. The estuarine alluvial deposits correspond to salt flats composed of mud and intervals of fine sand and silts, forming slightly elevated alluvial terraces. The thickness of the alluvial deposits could reach several hundred meters [10].

In the Balao area, the sands are poorly sorted, very asymmetrical towards coarse sizes, mesokurtic to very leptokurtic, unconsolidated, with common fragments of coal and phlogopite, rare fragments of resin, deposited under low energy conditions due to the tidal influence of the intertidal zone. The silts and sandy silts are poorly sorted, very asymmetrical towards fine sizes, platykurtic. The sedimentary environments of these sediments are associated with coastal channel types, transitional mangrove and subtidal estuary [13-14].

The Pallatanga fault has a NE-SW orientation and traverses the Gulf of Guayaquil and along Puná Island to the ocean trench [15]. East of Puná Island, there is the Jambelí system whose structures are dominated by the Puerto Balao fault with a NE-SW direction, marking the southern boundary of the Jambelí basin [16]. South of Balao, the Río Chico fault is present with a predominantly E-W trend and normal kinematics. The Figure 1 shows the geological setting in the areas near the epicenter of the Mw6.6 Balao earthquake and the Gulf of Guayaquil.

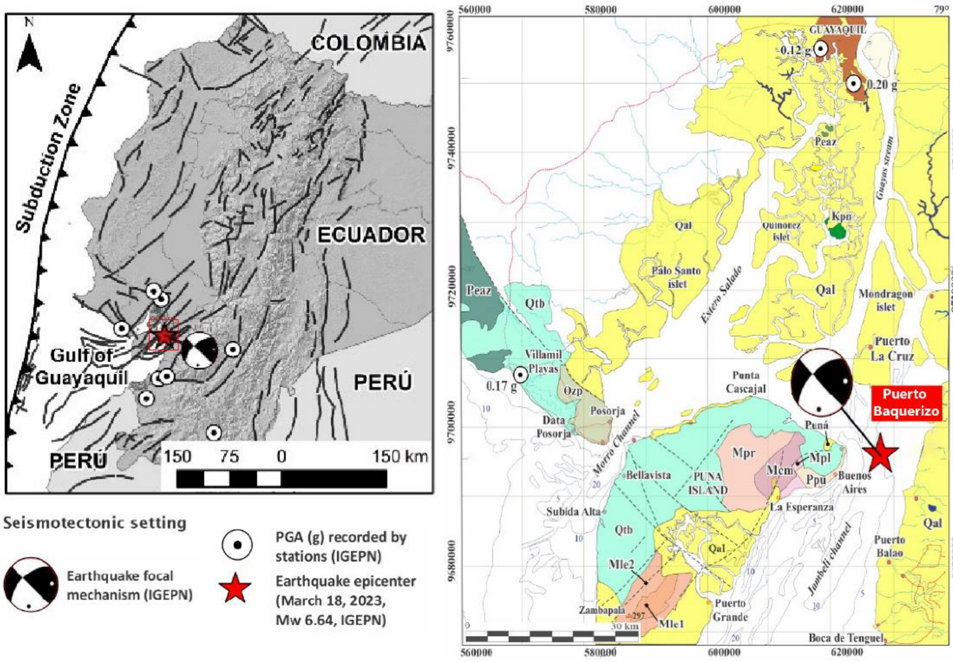

Figure 1 Overview map of the inner estuary of the Gulf of Guayaquil (modified from Aleman, [12])

3. Seismotectonic background and 2023 Mw6.6 Balao earthquake

The Gulf of Guayaquil, located on the southern coast of Ecuador bordering Peru, is subject to the dynamic deformation caused by the subduction of the Nazca plates, the continental segment of the Norandine Block and the South American plate [17]. In this seismic scenario, there are documented interplate subduction earthquakes with focal mechanisms associated to compression stresses (1901 Mw7.1 and 1942 Mw7.6 earthquakes), and intraplate associated with focal mechanisms associated to traction stresses (1913 Mw7.4 Zaruma earthquake) [18-19].

Another seismic scenario is associated with the deformation zone between the Norandino Block and the South American plate, where the mechanisms are associated to strike-slip vertical displacements [20] . The deepest focal distances can be between 60 to 70 km. A third seismic scenario is associated to geological faults with the potential to generate moderate earthquakes (between $6 \leq Mw \leq 7.1$) and peak ground accelerations (PGAs) ranging between 0.33 g and 0.36 g [21]. Many of these geological structures are associated with normal and strike-slip faults, where focal distances can be less than 16 km. The closest distance to the ruptures (Rrup) considered for seismic hazard analysis applied to the main Ecuadorian cities, should be considered between 32 to 15 km distances.

Chunga et al. [21] provides the cartography of the active geological faults with the potential to generate moderate to high earthquakes in the influence zone of the Gulf of Guayaquil. To estimate the moment magnitude (Mw) of the earthquake that could be generated by the faults identified by Chunga et al. [22], considering 100% and 60% of its seismic activation (according to the NEC-11 regulations; 2015), the Wesnousky model [23] has been used for each type of geological fault (Eq. 1 for strike slip fault and Eq. 2 for normal fault):

$$\mathrm{Mw} = 5.56 + 0.87 \cdot \mathrm{Log(Lf)} \tag{1}$$

$$\mathrm{Mw} = 6.12 + 0.47 \cdot \mathrm{Log(Lf)} \tag{2}$$

where Lf represents the length of the fault of interest.

Another intensity parameter evaluated by Chunga et al. [24] is the PGA in rock, applying the equation proposed by Fukushima & Tanaka [25]. These values of maximum accelerations in rocks are comparable with the seismic zoning map of Ecuador (Ecuadorian Construction Code NEC, 2011). The equation is detailed as follows:

$$PGA_{rock} = (10^{0.41M_e - log_{10}(H_f + 0.032*10^{0.41M_e})} - 0.0034H_f + 1.3)/980 \tag{3}$$

The historical earthquakes with higher magnitude close to the internal coast of the Gulf of Guayaquil, are: [a] Mw 5.7 July 9, 1653 with estimated depth less than 10 km; [b] Mw 6.5 June 11, 1787 with estimated depth 15 km, [c] Mw 6.2 March 12, 1962, [d] Mw 5.5 August 18, 1980 with estimated depth 15 km, [e] Mw 5.3 April 26, 1995; depth 19 km). [f] Mw 5.3 April 26, 1995; depth 19 km. The Mw 6.2 1961 earthquake with estimated hypocenter depth of about 33 km is considered an intraplate event. The earthquakes of March 12, 1962 (Mw 6.2) and March 18, 2023 (Mw6.6, depth of 68 km) are considered a horizontal shear mechanism, associated with the displacement between the Norandino block and the South American plate.

The recent 2023 Mw6.6 earthquake severely affected in the provinces of El Oro (129 affected and 78 destroyed buildings), Guayas (49 affected and 7 destroyed buildings), Azuay (14 affected and 4 destroyed buildings), and extent to Loja, Los Rios, Bolívar, Cañar and Chimborazo. In total 192 affected and 89 destroyed buildings have been documented, and at least 13 deaths and 484 injuries were recorded. The epicenter was located at the decimal degree coordinates of -2.752° N, -79.881° E, with a focal depth of 63 km, strike 135°, dip 88° and rake 148°.

In urban areas such as Puerto Baquerizo (a. in Figure *2*), Machala (b. in Figure *2*) and Mondragon Islet (c. in Figure *2*) clear evidence of earthquake-induced soil liquefaction was observed after the Mw6.6 Balao earthquake. The identified expressions of liquefaction include the presence of sand volcanoes, ground cracking and evidence of damage in structural and non-structural elements of buildings near the sites where the manifestation of ground liquefaction was observed.

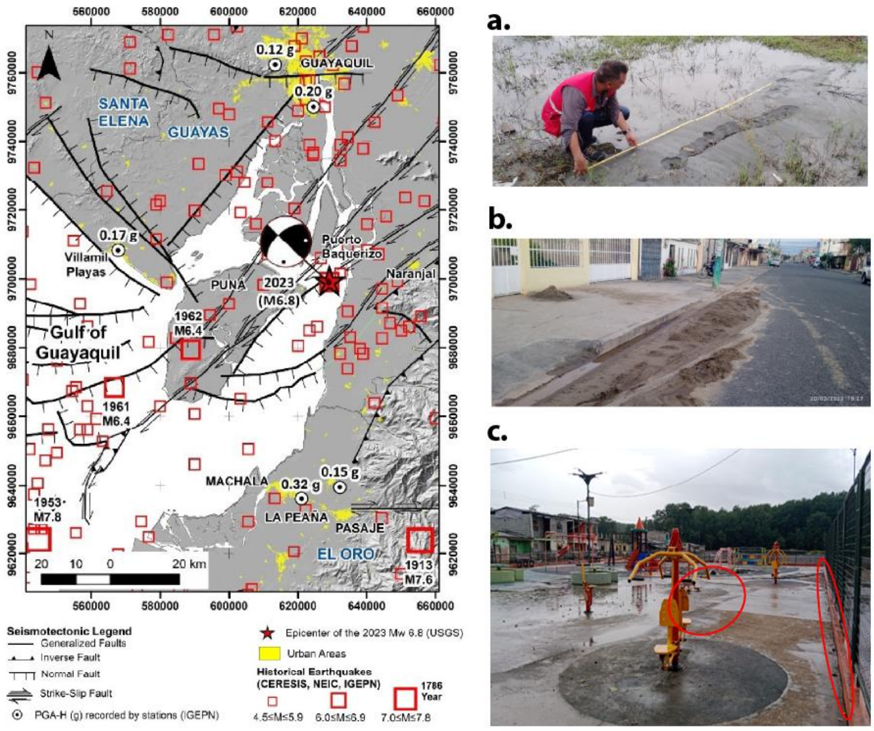

Figure 2 Seismotectonic map of the Gulf of Guayaquil; historical earthquakes nearby the site according to Regional Seismology Center for South America (CERESIS), National Earthquake Information Center (NEIC) and Geophysic Institute of the National Polytechnical School (IGEPN); 2023 Mw6.6 Balao earthquake epicenter reported by the United States Geological Surveys (USGS); maximum horizontal peak ground acceleration (PGA-H) recorded by the Ecuadorian Accelerograph Network Stations (IGEPN) in Balao earthquake

3.1. Grain size analysis

In order to study the composition and classification of the sandy material ejected to the surface in Puerto Baquerizo, grain-size analysis was carried out according to the ASTM C-136-01 [26]. The tests were performed on two samples recovered in different sand volcanoes. The samples of ejected material correspond to a non-plastic poorly graded silty sand (SP-SM according to the Unified Soil Classification System, USCS, [27] and a non-plastic poorly graded sand (SP), with fines content (FC) of 6.6% and 4.5%, respectively. As shown in Figure 3, between 85% and 90% of the sieved material corresponds to fine sand (0.075-0.425 mm of grain size), while a limited fraction of the samples corresponds to a medium sand (0.425-2 mm of grain size). The Table 1 summarizes the characteristic diameters of the 10%, 30% and 60% of the particles, namely D_{10}, D_{30} and D_{60} respectively, and the coefficient of uniformity (C_u) and of curvature (C_c).

Table 1 Grain-size properties of the ejected sand material in Puerto Baquerizo

Sample	**USCS**	**D_{10} (mm)**	**D_{30} (mm)**	**D_{60} (mm)**	**C_u (-)**	**C_c (-)**	**FC (%)**
Sample 1	SP-SM	0.082	0.122	0.187	2.28	0.97	6.63
Sample 2	SP	0.096	0.162	0.244	2.55	1.13	4.54

The material recovered from Puerto Baquerizo presents grain sizes between 2 and 5 times larger than the sand boils samples obtained in Boca de Briceño (central-coastal of Ecuador with ejecta classified as silty sand) after the liquefaction induced by the Mw7.8 Pedernales earthquake [7]. In the same way, the fines content measured in the soils recovered from Puerto Baquerizo is notably lower than that of the ejected sand in Boca de Briceño (FC > 35%).

The uniformity of the ejected sands in Puerto Baquerizo could be explained due to the pulse flows generated in the dikes and subsequent extrusion of the material to the surface during the liquefaction process [28]. Therefore, the granulometric distribution and the fines content observed in the material recovered on the surface may not be representative of the source layer.

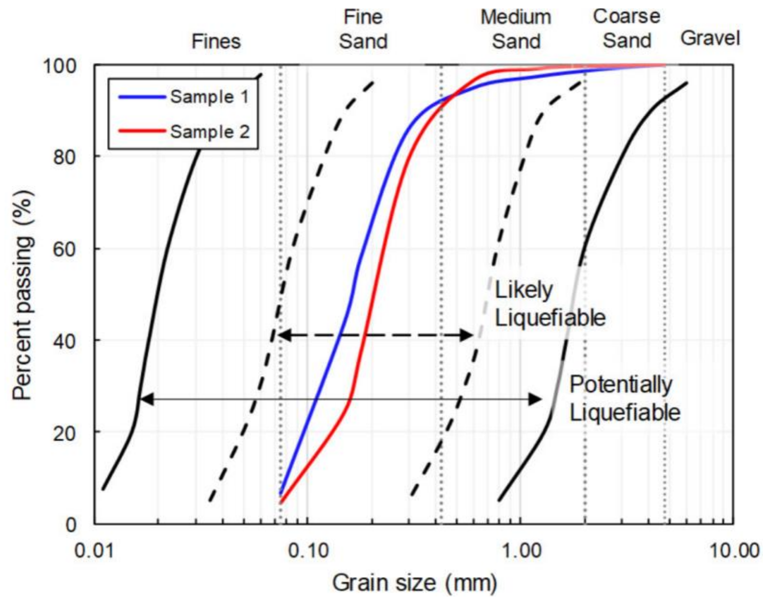

Figure 3 Grain size distribution of samples of ejected sand in Puerto Baquerizo and the boundaries of potentially liquefiable material from Tsuchida and Hayashi [29]

3.2. Morphological analysis

For morphological evaluation additional grain-size analyses were carried out in the present study. Samples were dry-sieved using sieves #30 (0.6 mm), #50 (0.3 mm), #80 (0.180 mm), and #100 (0.150 mm). Morphological and componentry analyses were conducted on the four grainsize ranges depicted in the high-resolution photo (…).

For morphological analyses, an average of 500 clasts were measured using Image-J software via image analysis to determine area, perimeter, major and minor axes, and circularity. Between the 70% and 80% of the soil particles analyzed corresponded to rounded grains with circularity coefficient between 0.70 and 0.90. The particles retained on sieves #80 and #100 had approximately 10% more rounded particles than the rest of the analyzed samples. Sands with uniform rounded particles are highly susceptible to liquefaction, since they tend to have higher void ratios and to develop greater volumetric deformations [30-31].

Component analyses were performed through point counting on high-resolution images taken under transmitted-light microscopy within the selected grain-size fraction. All samples contained a minimum of 500 clusters. Six main compositional categories were identified: Quartz (mainly as free crystals), Feldspar (principally as K-Feldspar), Metamorphic rock fragments, Volcanic rock fragments, Mica (muscovite), and Calcite fragments. The counting process was conducted using automatic particle selection through the Image-J program, with adjustments made to the image threshold to facilitate color-based segmentation of particles for each category. Results are presented in Figure 4 using the Q (quartz) + F (feldspars), L (siliciclastic lithics) and C (carbonate) diagram and in the Q (quartz), F (feldspars), and L (siliciclastic lithics) + C (carbonate) diagram.

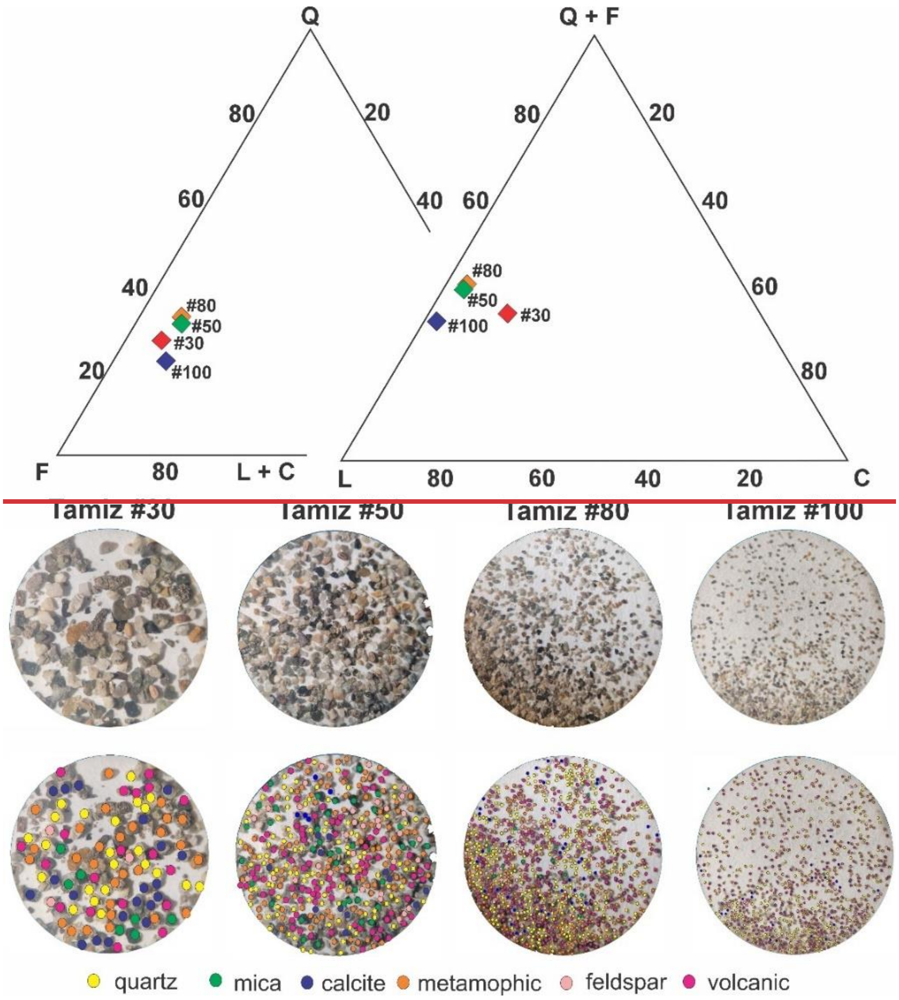

Figure 4 Ternary diagrams (Q, F, L+C and Q+F, L, C) showing the morphological composition of the ejected sand in Puerto Baquerizo

4. Site campaign

The site investigation program consisted of performing one SDMT test and one CPTu where the effects of liquefaction were most evident, close to the sand volcanoes shown in the **¡Error! No se encuentra el origen de la referencia.**. For the SDMT the corrected lift off (p_0) and 1.1 mm deformation pressures (p_1) were measured every 0.2 m up to 20 m depth, while the equilibrium pressure after deflation (p_2) was carried out at levels where the presence of materials with drained behavior was encountered, detecting the ground water table (GWT) at 1.8 m from the surface. The shear wave velocity (V_S)

measurements were carried out each 0.5 m up to 8 m depth, and each 1.0 m between 8 m and 17 m depth.

For the CPTu the cone resistance (q_c), sleeve friction resistance (f_s) and the pore pressure (u_2) were measured each 0.01 m until 20 m depth, identifying the GWT at 1.5 m. As well as in the SDMT, dissipation tests were carried out when the presence of drained materials was observed. The equilibrium hydrostatic pressures measured at the end of the dissipations confirmed the observed depth of the GWT at 1.5 m. The different GWT recorded by SDMT and CPTU can be due to the GWT seasonal fluctuation considering that the SDMT was performed in August 2023 while the CPTu in December 2023, in the beginning of the rainy season on the Ecuadorian coast.

The Figure 5 and Figure 6 shows the parameters measured and interpreted from both tests carried out. In particular Figure 5 plots the profile of SDMT parameters in terms of: the material index (I_D); the fines content (FC) according to Di Buccio et al. [33] ; the horizontal stress index (K_D); the corrected lift off pressure (p_0) and the 1.1 mm deflection pressure (p_1); the corrected equilibrium pressure after deflating (p_2) and the hydrostatic pore water pressure (u_0); and the shear wave velocity (Vs) measured in the SDMT and estimated from the DMT [34-35] and CPTu data [36]. For CPTu Figure 6 reports the following parameters: soil behavior type index (I_c); fines content (FC) according to Boulanger and Idriss [3] and Suzuki. [37]; corrected cone resistance (q_t); normalized friction ratio (Fr); and pore water pressure excess (u_2) and hydrostatic pore pressure.

By comparing the soil profiles, it can be noticed that there is a good agreement in the classification of the material determined by I_D from DMT and I_c from CPTu, identifying cohesive or cohesionless behaviors at similar depths. Both tests identify the presence of sandy layer with 3.9 m of thickness, underlying a cohesive crust. The beginning of the sandy layer is located at 2.6 m by the SDMT and at 2.9 m by the CPTu, while the end of the incoherent layer is located at approximately 6.5 m by both tests. Both tests identify that under the sandy layer there are fine intercalations of granular materials with cohesive layers up to 14 m depth. However, none of these intercalations has sufficient thickness to be considered a well-defined sandy geotechnical unit.

In the sandy interval I_D slightly ranges between 1.70 and 2.10, while K_D and V_S show a significant increase between 4.5 m and 6 m depth, reaching magnitudes between 6 and 7.5 for K_D and between 120 and 150 m/s for V_S. At the upper and lower boundaries of the sandy layer the K_D values tend to be between 3 and 4, while V_S is between 110 and 160 m/s.

On the other hand, for CPTu in the sandy layer I_c varies between 1.6 and 1.8 while q_t is between 2.3 and 5.5 MPa, and Fr is approximately 0.20%. The lowest values of the corrected cone penetration resistance (q_t) were measured in the same depth interval (between 2.5 m and 3.0 m depth) where the SDMT detected the lowest values of the horizontal stress index (K_D). However, from 4.2 m depth the resistance to penetration of the CPTu cone shows little variability, being 4 MPa the average magnitude. No marked peaks from CPTu are observed around 5 m depth, where maximums of K_D were estimated.

In order to approximate the fines content (FC) of the sandy materials prior to proceed to the liquefaction assessment, the estimations provided by the I_D-FC and the I_c-FC correlations were compared, observing a great variability. The Figure 5 shows that in the region where sandy material is detected, the I_D-FC model from Di Buccio et al. (2023) provides fines content between 25% and 40%. Instead Suzuki [37] at the same depth interval determines FC that vary slightly around 8% and 25%, while Boulanger and Idriss [3] indicate the presence of a clean sand, with fines content ranging between 0 to 25%, as is shown in the Figure 6.

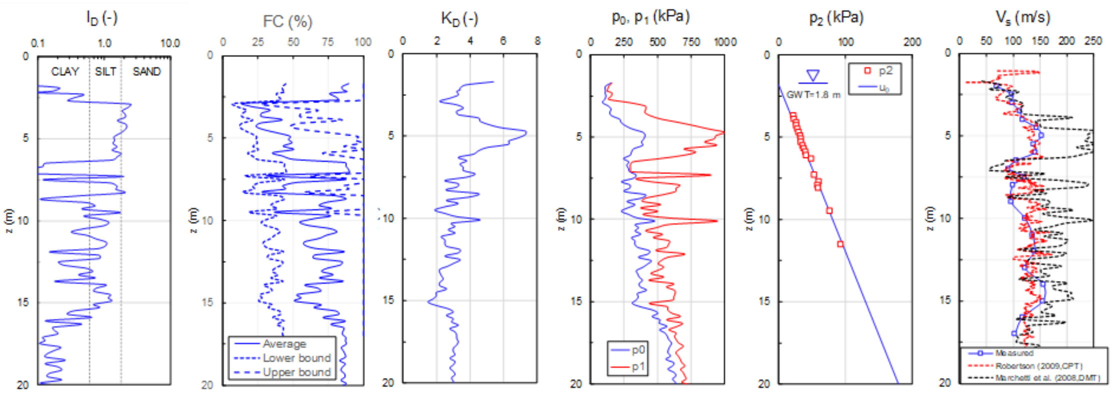

Figure 5 SDMT test results at Puerto Baquerizo liquefied site.

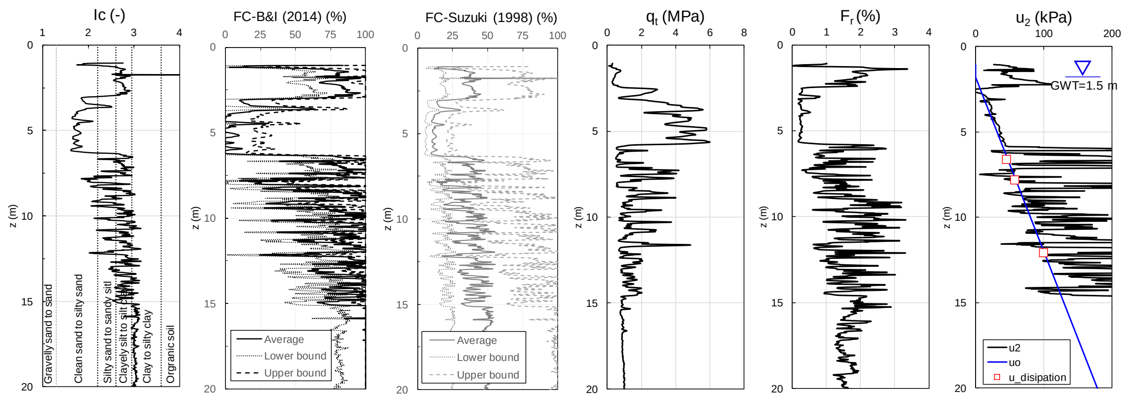

Figure 6 CPTu test results at Puerto Baquerizo liquefied site

5. Liquefaction potential assessment

5.1. Cyclic resistance ratio estimation

To calculate the cyclic resistance ratio ($CRR_{7.5}$) were selected a set of methodologies that use the information provided by the SDMT and CPTu tests as input. In general, the methods selected for the development of this case study are classified as follows: (i) methods based on the horizontal stress index (K_D) using only DMT information (Monaco et al. [38], Eq. 3; Tsai et al. [39], Eq. 4; Robertson et al. [40], Eq. 5; Marchetti [41], Eq. 6; Chiaradonna and Monaco [42], Eq. 6); (ii) methods based on the overburden corrected penetration resistances for clean sand (q_{c1Ncs}) using only CPTu information (Idriss and Boulanger [2], Eq. 8; Boulanger and Idriss [3], Eq. 9); (iii) methods that combine the use of the DMT and CPTu information (Marchetti [41], Eq. 10) and (iv) methods that use the overburden corrected shear wave velocity (V_{S1}, Andrus and Stokoe [43], Eq. 11; Kayen et al. [44], Eq. 12).

$$\mathrm{CRR}_{7.5} = 0.0107 \cdot \mathrm{K}_\mathrm{D}^3 - 0.0741 \cdot \mathrm{K}_\mathrm{D}^2 + 0.2169 \cdot \mathrm{K}_\mathrm{D} - 0.1306 \tag{3}$$

$$\mathrm{CRR}_{7.5} = \exp\left[\left(\frac{\mathrm{K_D}}{8.8}\right)^3 - \left(\frac{\mathrm{K_D}}{6.5}\right)^2 + \left(\frac{\mathrm{K_D}}{2.5}\right) - 3.1\right] \tag{4}$$

$$\mathrm{CRR}_{7.5} = 93 \cdot (0.025 \cdot \mathrm{K_D})^3 + 0.08 \tag{5}$$

$$\mathrm{CRR}_{7.5} = \exp[0.2192 \cdot \mathrm{K}_\mathrm{D}^4 - 0.3125 \cdot \mathrm{K}_\mathrm{D}^3 + 0.3731 \cdot \mathrm{K}_\mathrm{D}^2 + 0.0462 \cdot \mathrm{K}_\mathrm{D} - 3] \tag{6}$$

$$\mathrm{CRR}_{7.5} = \exp\,(0.0011097 \cdot \mathrm{K}_\mathrm{D}^4 - 0.0057 \cdot \mathrm{K}_\mathrm{D}^3 + 0.00062 \cdot \mathrm{K}_\mathrm{D}^2 + 0.22 \cdot \mathrm{K}_\mathrm{D} - 2.8) \tag{7}$$

$$\mathrm{CRR}_{7.5} = \exp\left[\left(\frac{q_{c1n\,cs}}{540}\right) + \left(\frac{q_{c1n\,cs}}{67}\right)^2 - \left(\frac{q_{c1n\,cs}}{80}\right)^3 + \left(\frac{q_{c1n\,cs}}{114}\right)^4 - 3\right] \tag{8}$$

$$\mathrm{CRR}_{7.5} = \exp\left[\left(\frac{q_{c1n\,cs}}{113}\right) + \left(\frac{q_{c1n\,cs}}{1000}\right)^2 - \left(\frac{q_{c1n\,cs}}{140}\right)^3 + \left(\frac{q_{c1n\,cs}}{137}\right)^4 - 2.80\right] \tag{9}$$

$$\mathrm{CRR}_{7.5} = [(\mathrm{CRR}_{7.5} \text{ from } q_{c1n\,cs}) \cdot (\mathrm{CRR}_{7.5} \text{ from } K_D)]\text{^}0.5 \tag{10}$$

$$\mathrm{CRR}_{7.5} = \left[0.022 \cdot \left(\frac{V_{s1}}{100}\right)^2 + 2.8 \cdot \left(\frac{1}{V_{s1}^* - V_{s1}} - \frac{1}{V_{s1}^*}\right)\right] \tag{11}$$

$$\mathrm{CRR}_{7.5} = \exp\left\{\left[(0.0073 \cdot V_{s1})^{2.8011} - 2.6168 \cdot \ln(M_w) - 0.0099 \cdot \ln(\sigma'_{vo}) + 0.0028 \cdot FC - 0.4809 \cdot \Phi^{-1}(P_{L)}\right]/1.946\right\} \tag{12}$$

The DMT data were filtered to calculate the $\mathrm{CRR}_{7.5}$ only in the soils where $I_D \geq 1.2$, where $I_D = 1.2$ represents the boundary between silts and sandy silt according to Marchetti and Crapps [45], while the CPTu data were filtered for $I_c \leq 2.6$, since $I_c = 2.6$ is approximately the threshold between clayey silt to silty clay and silty sand to sandy silt. However, although models that correlate FC with I_D and Ic are widely used in geotechnical engineering practice, there is large uncertainty regarding whether these values adequately fit to the FC of Ecuadorian soils. No research has been developed to calibrated these models with FC from laboratory tests. Therefore, there is a possibility that certain potentially liquefiable materials are not being adequately considered within the present analysis, especially those with I_D and Ic slightly less than 1.2 and higher than 2.6, respectively. Further research it is necessary in order to calibrate the models of Suzuki [37], Boulanger and Idriss [3] and Di Buccio et al. [33].

The DMT methodologies were developed by the authors considering the close relationship between the K_D and the parameters directly related to the liquefaction potential such as the relative density (D_r), the in-situ earth pressure coefficient (K_0), and the overconsolidation ratio (OCR, [38, 46-50]);. Most of these expressions were derived using existing $\mathrm{CRR}_{7.5}$ models available from Standard Penetration Test (SPT) or Cone Penetration Test (CPT), and replacing their variables (overburden corrected penetration resistances for clean sand, i.e. N_{160cs} for SPT and q_{c1Ncs} for CPT) with the equivalent values from the $K_{D.}$

The models proposed by Boulanger and Idriss [3] were developed with robust in situ background, including in the database recent historical cases of liquefaction assessment in events such as 2010-2011 Canterbury earthquake sequence, 2011 Mw9 Tohoku earthquake.

Considering the availability of CPTu and SDMT data, carried out at nearby sites, the Marchetti [41] q_{c1Ncs}-K_D based model was introduced into the analysis. This method defines the cyclic resistance rate as the geometric mean between the resistances calculated from methods based on cone resistance (Boulanger and Idriss [2], according to Marchetti,

[41]) and those determined by the K_D-based method, as is detailed in the Eq.9. Since the frequency of data acquisition diverges between the DMT and CPTu tests (DMT data every 0.20 m, and CPTU data every 0.01 m), the q_{c1Ncs} values were averaged around the levels where the DMT data were obtained. In this way, the average cyclic resistance ratio calculated with Idriss and Boulanger [2] takes into consideration the behavior of the materials above and below each depth of analysis. For this method, only those materials with $I_D \geq 1.20$ and an average $I_c \leq 2.6$ were considered as soils with sand-like behavior.

Finally, regarding the V_S-based simplified methods the Andrus and Stokoe [43] includes a shear wave velocity value corrected for the fines content (V_S*), while the Kayen et al. [44] model includes also a probabilistic term, which is the inverse cumulative normal distribution $\Phi^{-1}(P_L)$, defined to a liquefaction probability (P_L) of 15%. The FC estimates were derived from the Di Buccio et al. [33] model, as a differentiation criterion between soils with sand-like or clay-like behavior, as well as for the calculation of the $CRR_{7.5}$ from Andrus and Stokoe [43] and Kayen et al. [44] equations.

5.2. Cyclic stress ratio estimation

The cyclic stress ratio corrected for a Mw7.5 and an overburden stress of 1 atm ($CSR_{7.5, 1\,atm}$) was determined by applying the simplified procedure proposed by Seed and Idriss [51]. This model indicates that the $CSR_{7.5, 1atm}$ could be determinate from the following expression:

$$\mathrm{CSR}_{7.5,1\mathrm{atm}} = 0.65 \cdot \left(\frac{\mathrm{a}_{\max}}{\mathrm{g}}\right) \cdot \mathrm{r_d} \cdot \left(\frac{\sigma_{\mathrm{vo}}}{\sigma'_{\mathrm{vo}}}\right) \cdot \frac{1}{\mathrm{MSF} \cdot \mathrm{K}_\sigma} \tag{13}$$

Where the term a_{max} is the maximum horizontal acceleration at surface, g is the gravity, r_d is the shear stress reduction coefficient, MSF is the magnitude scale factor, K_σ is the overburden correction factor, while σ_{v0} and σ'_{v0} represents the total and effective stress. The σ'_{v0} was computed assuming a safe GWT at 1.5 m. This assumption takes into account that March (when the earthquake occurred) is part of the rainy season in the Coast of Ecuador, and the test was performed in months where low levels of precipitations exist in the area.

For the CPT-based and DMT+CPT-based methods, the r_d and K_σ values were estimated according to Idriss and Boulanger [2]. Since there are no models that correlate K_σ with the parameters measured or interpreted from the DMT, the values calculated of K_σ from the CPTu were considered for the estimation of the seismic demand for the DMT-based methods. While the magnitude scale factor (MSF) was computed using the

Boulanger and Idriss [3] relationships with the $q_{c1n\ cs}$ calculated from the results of the CPTu test.

The Andrus and Stokoe [44] method was synthesized using the stress reduction coefficient (r_d) and magnitude scale factor (MSF) relationships recommended by the NCEER Workshop [52]. To be consistent with the considerations made by the author, the same relationships of the NCEER Workshop model [52] were used for the calculation of the seismic demand in the evaluation of the liquefaction potential based on the Andrus and Stokoe method [43]. The overburden correction factor (K_σ) was assumed equal to 1 for the liquefaction assessment from Andrus and Stokoe [43]. For the Kayen et al. [44] method, the specific relationships proposed by the author were used to calculate the stress reduction coefficient and the magnitude scale factor.

The last important issue to estimate the cyclic stress ratio ($CSR_{7.5,\ 1\ atm}$) was the quantitative evaluation of the maximum horizontal acceleration during the Mw6.6 earthquake. The estimation in Puerto Baquerizo was carried out by applying the Ground Motion Prediction Equations (GMPEs) proposed by different authors for in-slab earthquakes. This decision was made since the closest station of the Ecuadorian Accelerograph Network to the study site are between 60 and 70 km away, and with slightly greater epicentral distances. Therefore, their measurements were not considered representative of the accelerations induced in Puerto Baquerizo. However, by having both the epicentral distance and the recorded horizontal accelerations well documented, the information provided by the Ecuadorian Accelerograph Network represented an important database for the validation of the predictions made by the GMPEs.

The Table 2 summarizes the peak horizontal ground acceleration (a_{max}) recorded by the closest accelerograph stations, the estimated epicentral distance (R) and the referential geological setting for each site.

Table 2 Ground motions recorded by the Ecuadorian Accelerograph Network stations during the Mw6.6 Balao Earthquake

ID Station	**R (km)**	**a_{max} (g)**		**Geological Setting**
		N-S	**E-W**	
ACH1	53.2	0.32	0.19	Cuaternary marine terraces
ACH2	53.6	0.15	0.09	Piroclastics materials / Andesite / Rhyolite

GYKA	62.5	0.2	0.16	Cuaternary marine terraces
AC07	73.2	0.12	0.12	Guayaquil Formation (siltstones/shales)
ARNL	81.7	0.18	0.03	Marine terraces / Alluvial Deposits
APLA	48.9	0.17	0.1	Tablazo Formation (sandstones)
ACUE	115	0.05	0.07	Alluvial Deposits / Sandstones
ALJ1	156.8	0.02	0.05	Quilloaco Group (siltstones)

The models selected for the evaluation were: Youngs et al. [53], Atkinson and Boore [54] and Zhao et al. [55]. The GMPEs proposed by Atkinson and Boore [54] and Zhao et al. [55] include site factors to evaluate the effect of the dynamic properties of the deposit on the expected seismic intensities. In both cases, the chosen site parameters correspond to the most unfavorable ground condition, which meant, NEHRP E or NEHRP F type soils, with average shear-wave velocity for the upper 30 m depth (V_{S30}) less than 200 m/s.

An important difference to note is that the models proposed by Youngs et al. [53] and Atkinson and Boore [54] estimate the maximum horizontal acceleration in a random component, while Zhao et al. [55] estimates the geometric mean (geomean) of the two horizontal acceleration components. Then, in order to validate the intensities calculated by the selected models, the maximum acceleration of the two components (blue squares in Figure 7) and the geometric mean acceleration (grey rhombuses in Figure 7) were plotted together with the predicted acceleration from the GMPEs, as shown in the Figure 7. A good correlation was observed between the predicted accelerations and those measured by the Ecuadorian Accelerograph Network. Therefore, their use for the estimation of the maximum horizontal acceleration (a_{max}) in Puerto Baquerizo was considered appropriate.

The epicentral distance (R) to Puerto Baquerizo site is approximately 35 km. For this distance the models predict accelerations between 0.28g and 0.48 g, according to the models of Youngs et al. [53] and Zhao et al. [55], respectively. Finally, the Atkinson and Boore [54] equation determined a horizontal acceleration of 0.38g. For the liquefaction potential analysis, the geometric mean of the three calculated accelerations was used, which means, 0.35g.

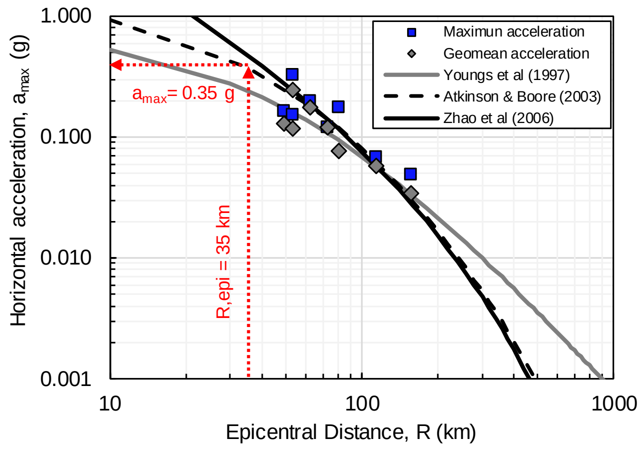

Figure 7 Maximum horizontal acceleration prediction in Puerto Baquerizo in Mw6.6 Balao earthquake

5.3.Results and discussions

The cyclic stress ratio ($CSR_{7.5,\ 1atm}$) was estimated between 0.30 and 0.37 using the methodology proposed by Boulanger and Idriss [3] for the sand-like layers (black and white dots in Figure 9a, Figure 9b and Figure 9c). Through Youd et al. ([52], purple dots in Figure 9d) the cyclic stress ratios ($CSR_{7.5,\ 1\ atm}$) were determined between 0.29 and 0.35. These values represent between 15% and 30% less than that calculated from Boulanger and Idriss [3]. This fact is more noticeable for the results obtained from Kayen et al. [44] which report cyclic stress ratios between 0.25 to 0.27 for the sand-like soils (red dots in Figure 9d).

Regarding to soil liquefaction resistance evaluation, all the methods determine the $CRR_{7.5}$ between 0.10 and 0.25. Hence, the factors of safety against liquefaction were calculated between 0.25 and 0.60 for the sand-like deposits, as shown in Figure 8. According to these results, almost all the granular materials identified in the investigation program between 2.6 m and 6.5 m are classified as liquefiable.

However, the K_D-based methods and the Andrus and Stokoe [43] Vs-based method, report a substantial increase in the resistance calculated between 4.9 and 5.3 m depth, turning these materials as non-liquefiable for a Mw6.6 event. This condition is fundamentally related by the increase in the values of K_D and Vs up to magnitudes of 7.5 and 215 m/s at this depth, respectively. This behavior is not detected in the evaluation of the $CRR_{7.5}$ by the CPT, the DMT+CPT and the Vs-based methods, identifying a continuous liquefiable layer between 2.7 and 6.3 m, and representing more conservative scenarios.

A first approximation of the severity of liquefaction was carried out by evaluating the Liquefaction Potential Index (LPI) proposed by Iwasaki et al. [56]. Typically, the estimated LPIs were ranging between 14 and 17 for the K_D-based methods, corresponding to a very high susceptibility to liquefaction. These results are consistent with the LPI calculated from the DMT+CPT Marchetti [41], the CPT and the V_S methods, where the calculated indices were between 17 and 21.8. Only in the evaluation from Monaco et al. [38] the site is classified in a lower category of severity.

An important observation about the results is that although the demand determined from Kayen et al. [44] is 25% lower than that determined by Boulanger and Idriss [3], the same difference is not observed with regard to safety factors and liquefaction potential indices compared to the other selected methods.

From the observed distribution of the LPI with depth, it could be highlighted that all evaluation methods agree that around the 70% of the contribution to the total LPI is generated between 2.7 m to 6.3 m. On the other hand, the contribution to the LPI below 9.5 m is practically negligible. The fines content in the material ejected to the surface after the Balao earthquake aligns with the average fines content estimated by Boulanger and Idriss [3]. It also matches the lower bound of the estimated values using Suzuki [37], considering this formula was calibrated in regions with higher liquefaction potential.

Therefore, considering: (i) the calculated safety factors, (ii) the distribution of the liquefaction potential index and (iii) the similarity in the fines content estimated, it can be deduced that the source layer of the liquefaction expressions observed at surface after the Balao earthquake was precisely the non-cohesive material located between 2.7 m and 6.3 m.

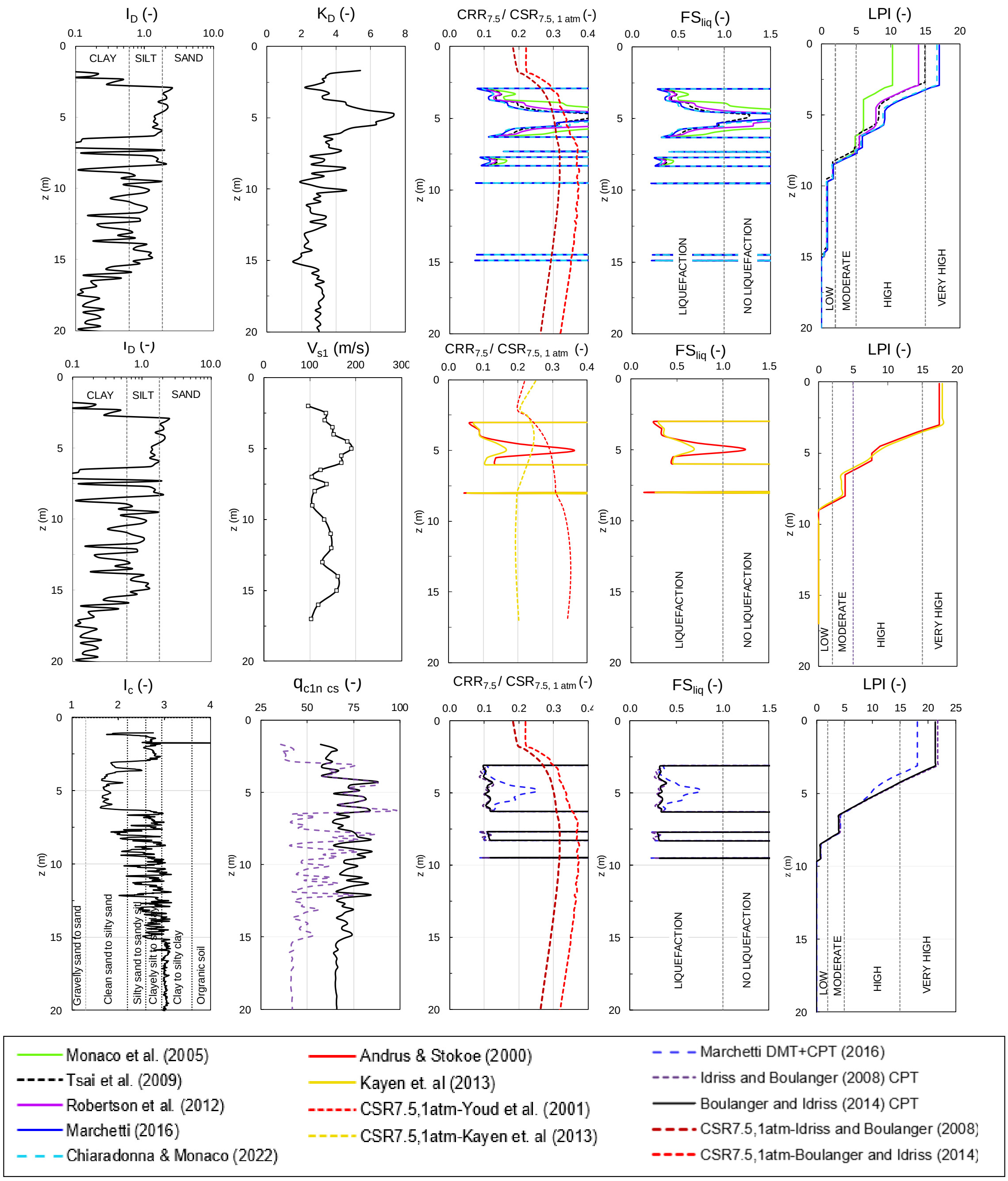

Figure 8 Liquefaction assessment results using: K_D-based methods (DMT), Vs-based methods (SDMT), qc-based methods (CPTu) and K_D-q_c-based methods (DMT+CPTu)

In order to validate the correlation of the results with the observed damages, additional parameters were determined to characterize the severity of liquefaction, such as: Ishihara-inspired Index (LPI_{ish}; Maurer et al. [57]), Post liquefaction volumetric deformation (S_{vol}; Zhang et al. [58]), Liquefaction Severity Number (LSN; Tonkin and Talylor, [59]) and the Induced Damage Measurement (I_{AM}; Chiaradonna and Flora, [60]) Since the computation of LPI_{ish} and I_{AM} directly involves the thickness of the non-liquefiable material above the source liquefaction layer, 2.7 m and 2.9 m were considered as the thickness of non-liquefiable material in the calculation of LPI_{ish} and I_{AM} for the SDMT and CPTu methods, respectively. Additionally, in order to apply the Zhang et al. [58] methodology for the SDMT derived methods to estimate post liquefaction volumetric deformation, averages of the qc1ncs calculated from the CPTu data were taken around each depth where SDMT data was available.

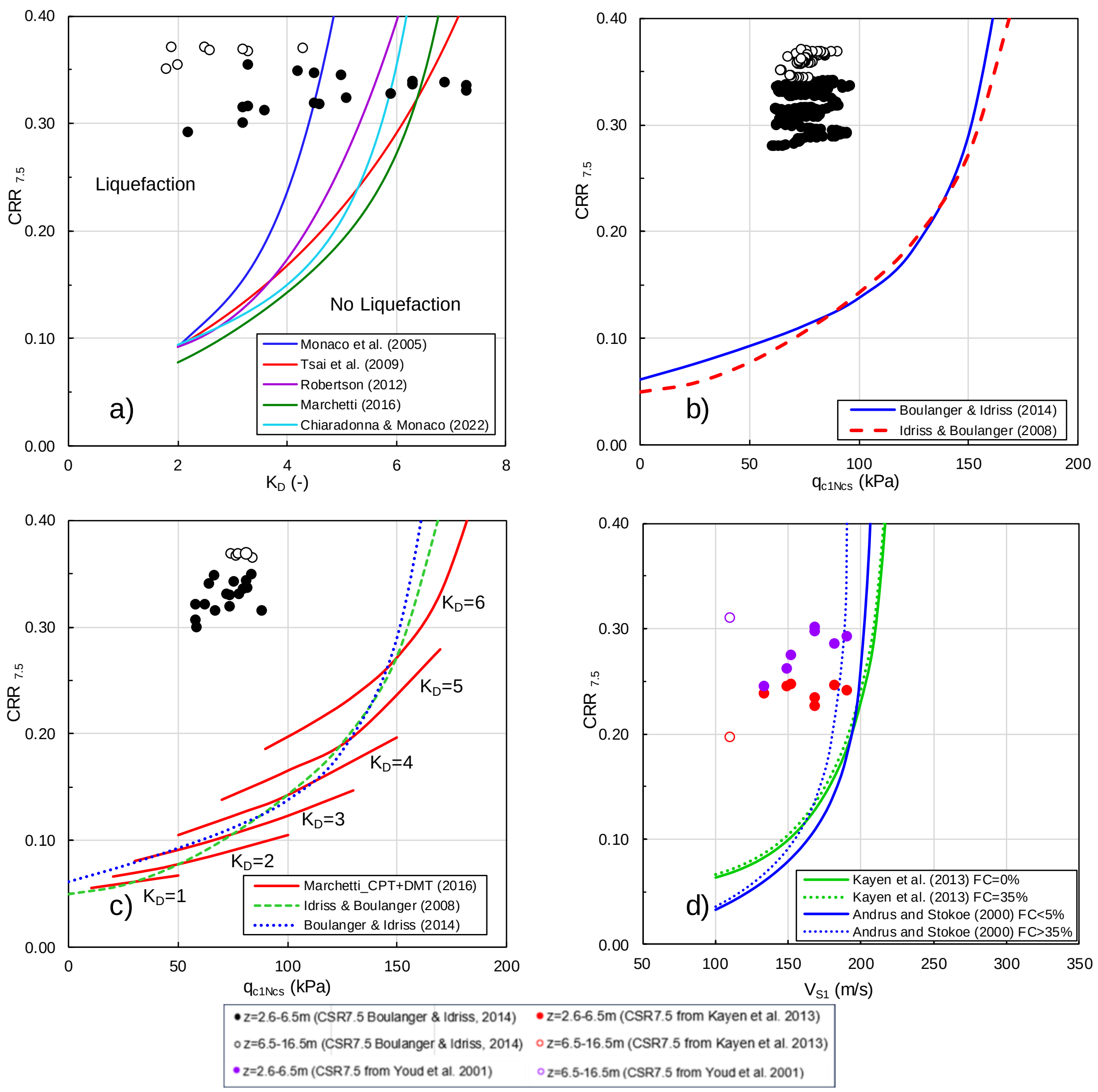

Figure 9 Cyclic resistance Ratio ($CRR_{7.5}$) curves for: a) K_D-based, b) qc-based, c) qc+ K_D-based and d) Vs-based methods, and their relation with the predicted Cyclic stress ratio ($CSR_{7.5,\ 1atm}$, from Boulanger & Idriss, [3]) in cohesiveness (data filtered for I_D>1.20, Ic<2.60 and FC>50%)

Table 3 Liquefaction Potential Index for Puerto Baquerizo estimated from SDMT and CPT test results

Method of assessment	**LPI (-)**	**LPI_{ish} (-)**	**S_{vol} (cm)**	**LSN (-)**	**I_{AM} (-)**
Monaco et al. (2005)	10.3	6.9	9.9	18.8	0.59
Tsai et al. (2009)	15	10.5	13.5	26.5	0.92
Robertson (2012)	14	9.9	12.3	24.1	0.77
Marchetti K_D-based (2016)	17	11.8	13.7	29	0.88
Chiaradonna and Monaco (2022)	16.6	11.9	13.4	27.5	0.84
Idriss and Boulanger CPT-based (2008)	21.8	15.3	18.7	32.6	0.85
Boulanger and Idriss CPT-based (2014)	21.4	15.1	18.1	31.9	0.85
Marchetti CPT+DMT (2016)	18.2	12.4	13.4	27.3	0.8
Andrus and Stokoe (2000)	17.5	13.7	12.1	27	0.85
Kayen et al. (2013)	17.9	13.9	13.4	30.1	0.92

The Table 3 summarizes all the severity indices determinate for each evaluation methodology. The results of LPI_{ish} and I_{AM} indicate that the severity of liquefaction would be between "High" to "Very high", that is, a lower expected impact of liquefaction compared to the results of the Liquefaction Potential Index. This fact implies that the presence of the cohesive layer above the liquefiable stratum mitigates importantly the effects of the liquefaction at surface.

On the other hand, the volumetric deformations were determined in the order of 9.9 cm to 18.7 cm. The q_c-based and K_D-q_c-based are the methods which calculated the highest levels of deformation, being Idriss and Boulanger [2] the model by which the maximum volumetric deformation were determinated. There is no information about the condition of site prior to the Balao earthquake, then it is not possible to verify whether the calculated settlement levels are related to what was observed on site.

The calculated Liquefaction Severity Number (LSN) values range between 18.8 and 40, which corresponds to moderate to severe expressions of liquefaction as a consequence of the Balao earthquake. According to Tonkin and Taylor [59], zones with moderate to severe expressions of liquefaction are characterized by the presence of sand volcanoes and the development of deformations that could generate some structural damage. This description agrees with what was observed at the study site, where the presence of sandy material at surface and cracks in structural and non-structural elements in buildings close to the sites where the liquefaction was evident could be observed.

6. Conclusions

The grain-size analysis carried out on samples recovered from sand boils in Puerto Baquerizo indicates that the material corresponds to non-plastic poorly graded silty sand (SP-SM) and a non-plastic poorly graded sand (SP), with fines content (FC) between 4% and 6%. The morphological and componentry evaluation determined that around 80% of the particles studied correspond to uniform rounded grains, composed mainly of Quartz, K-Feldspar, Mica, Calcite and fragments of volcanic and metamorphic rocks.

The results of the liquefaction assessment through methods based on SDMT and CPTu indicate that Puerto Baquerizo has a “High” to “Very High” liquefaction potential. This designation is consistent with the observed damage levels and expressions of surface liquefaction in Puerto Baquerizo after the 2023 Mw6.6 Balao earthquake.

From the calculated safety factors and the distribution of the different Liquefaction Potential Indices, it is deduced that the source layer of the liquefaction manifestations is a 3.9 m thickness sandy layer, identified by the SMDT an CPTu approximately 2.6 m below the surface. The estimation of fines contents (FC) based on correlations with the Material Index (I_D) and the Soil Behavior Type Index (I_c) are higher than those measured in the samples recovered at surface after the 2023 Mw6.6 Balao earthquake. However, this difference could be explained through the sorting of particles diameters during the material ejection process. More research is necessary to better understand the relationship between the fines content of the liquefaction source layers and the composition of the materials that are observed on the surface.

This work contributes to the understanding of the liquefaction phenomenon in Quaternary soils of the Ecuadorian coast, and seems to corroborate the applicability of different methodologies based on CPTu and SDMT to predict the potential and severity of liquefaction in one of the most seismically active areas in the world.

References

[1] Cetin, K., Seed, R., Der Kiureghian, A., Tokimatsu, K., Harder, L., Kayen, R., & Moss, R. (2004). Standard penetration test-based probabilistic and deterministic assessment of seismic soil liquefaction potential. Journal of Geotechnical and Geoenvironmental Engineering.

[2] Idriss, I., & Boulanger, R. (2008). Soil Liquefaction during Earthquakes. Earthquake Engineering Research Institute.

[3] Boulanger, R., & Idriss, I. (2014). CPT and SPT based liquefaction triggering procedures.

[4] GEER-ATC. (2016). Earthquake Reconnaissance 2016 Muisne, Ecuador Earthquake. GEER Report-049. https://doi.org/10.5072/FK2833T22B

[5] Chunga, K., Mulas, M., & Garcés, D. (2016). Geología de Terremotos y Tsunami (ECUADOR). https://www.researchgate.net/publication/309478442

[6] Vera Grunauer, X., Lopez-Zhindon, S., Ordoñez, J., & Chavez, M. (2019). Liquefaction case histories after the 2016 megathrust Pedernales earthquake in Ecuador. Earthquake Geotechnical Engineering for Protection and Development of Environmental and Constructions. https://www.researchgate.net/publication/341090265

[7] Salocchi, A. C., Minarelli, L., Lugli, S., Amoroso, S., Rollins, K. M., & Fontana, D. (2020). Liquefaction source layer for sand blows induced by the 2016 megathrust earthquake (Mw 7.8) in Ecuador (Boca de Briceño). Journal of South American Earth Sciences, 103. https://doi.org/10.1016/j.jsames.2020.102737

[8] AMOROSO ET AL 2021

[9] Ortiz-Hernández, E., Chunga, K., Toulkeridis, T., & Pastor, J. L. (2022). Soil Liquefaction and Other Seismic-Associated Phenomena in the City of Chone during the 2016 Earthquake of Coastal Ecuador. Applied Sciences (Switzerland), 12(15). https://doi.org/10.3390/app12157867

[10] IIGE,2016

[11] Dunkley, P., & Gaibor, A. (1997). Geology of the Cordillera Occidental of Ecuador between 2 00'and 3 00'S. CODIGEM-BGS, Quito, Ecuador.

[12] Alemán A. (2000) Progreso Basin. 223 p. {9}

[13] Chunga 2002

[14] Soledispa, B. (1987). Estudio de las características sedimentológicas del área comprendida entre Ancon y el Canal del Morro (Golfo de Guayaquil).

[15] Dumont, J. F., Santana, E., Vilema, W., Pedoja, K., Ordonez, M., Cruz, M., ... & Zambrano, I. (2005). Morphological and microtectonic analysis of quaternary deformation from puná and santa clara islands, gulf of guayaquil, Ecuador (South America). Tectonophysics, 399(1-4), 331-350.

[16] Witt, C., Bourgois, J., Michaud, F., Ordoñez, M., Jiménez, N., & Sosson, M. (2006). Development of the Gulf of Guayaquil (Ecuador) during the Quaternary as an effect of the North Andean block tectonic escape. Tectonics, 25(3).

[17] Aizprua, C., Witt, C., Brönner, M., Johansen, S. E., Barba, D., & Hernandez, M. J. (2020). Forearc crustal structure of Ecuador revealed by gravity and aeromagnetic anomalies and their geodynamic implications. Lithosphere, 2020(1), 2810692.

[18] Manchuel, K., Régnier, M., Béthoux, N., Font, Y., Sallarès, V., Díaz, J., & Yepes, H. (2011). New insights on the interseismic active deformation along the North Ecuadorian–South Colombian (NESC) margin. Tectonics, 30(4).

[19] Collot, J. Y., Proust, J. N., Nocquet, J. M., Martillo, C., Michaud, F., Lebrun, J. F., ... & Ratzov, G. (2022). From long-to short-term inter-plate coupling at the subducted Carnegie Ridge crest, offshore Central Ecuador. Journal of Geophysical Research: Solid Earth, 127(8), e2022JB024192.

[20] Mora et al 2015

[21] Chunga, K., Livio, F. A., Martillo, C., Lara-Saavedra, H., Ferrario, M. F., Zevallos, I., & Michetti, A. M. (2019). Landslides triggered by the 2016 Mw 7.8 Pedernales, Ecuador earthquake: Correlations with ESI-07 intensity, lithology, slope and PGA-h. Geosciences, 9(9), 371.

[22] Chunga et al. (2008)

[23] Wesnousky, S. G. (2008). Displacement and geometrical characteristics of earthquake surface ruptures: Issues and implications for seismic-hazard analysis and the process of earthquake rupture. Bulletin of the Seismological Society of America, 98(4), 1609-1632.

[24] Chunga, K., Matos, F., Mulas, M., Ochoa, F. (2018). "Characterization of seismogenetic crustal faults in Gulf of Guayaquil, Ecuador". Andeand Geology. Vol. 46, No.1. ISSN 0718-7092.

[25] Fukushima, Y., & Tanaka, T. (1990). A new attenuation relation for peak horizontal acceleration of strong earthquake ground motion in Japan. In Bulletin of the Seismological Society of America (Vol. 80, Issue 4). https://www.researchgate.net/publication/279901672

[26] American Society for Testing Materials. (2006). Standard Test Method for Sieve Analysis of Fine and Coarse Aggregates. ASTM-C136-06. https://doi.org/10.1520/C0136-06

[27] American Society for Testing Materials. (2017). Classification of Soils for Engineering Purposes – Unified Soil Classification System. ASTM-D2487-17. https://doi.org/10.1520/D2487-17

[28] Fontana, D., Amoroso, S., Minarelli, L., & Stefani, M. (2019b). Sand liquefaction induced by a blast test: New insights on source layer and grain-size segregation mechanisms (Late Quaternary, Emilia, Italy). Journal of Sedimentary Research, 89(1), 13–27. https://doi.org/10.2110/jsr.2019.1

[29] Tsuchida and Hayashi

[30] Kramer Steven. (1996). Geotechnical Earthquake Engineering (First). Prentice-Hall inc.

[31] Mitchell, J. K., Soga, K. (2005). Fundamentals of soil behavior. Third Edition. Jhon Wiley & Sons, Inc. New Jersey.

[32] Lugli, S., Marchetti S., & Fontana D. (2007). Alluvial sand composition as a tool to unravel late Quaternary sedimentation of the Modena Plain, northern Italy. Geological Society of America Special Papers, 420, 57–72.

[33] Di Buccio, F., Comina, C., Fontana, D., Minarelli, L., Vagnon, F., & Amoroso, S. (2023). Fines content determination through geotechnical and geophysical tests for liquefaction assessment in the Emilia alluvial plain (Ferrara, Italy). Soil Dynamics and Earthquake Engineering, 173. https://doi.org/10.1016/j.soildyn.2023.108057

[34] Marchetti, S., Monaco, P., Totani, G., & Marchetti, D. (2008). In Situ Tests by Seismic Dilatometer (SDMT). 292–311. https://doi.org/10.1061/40962(325)7

[35] Monaco, P., de Magistris, F. S., Grasso, S., Marchetti, S., Maugeri, M., & Totani, G. (2011). Analysis of the liquefaction phenomena in the village of Vittorito (L'Aquila). Bulletin of Earthquake Engineering, 9(1), 231–261. https://doi.org/10.1007/s10518-010-9228-0

[36] ROBERTSON 2009

[37] Suzuki, Y. (1998). Correlation between SPT and seismic CPT. In Proc. of the First International Conference on Site Characterization (Vol. 2, pp. 1375-1380).

[38] Monaco, P., Marchetti, S., Totani, G., & Calabrese, M. (2005). Sand liquefiability assessment by Flat Dilatometer Test (DMT).

[39] Tsai, P. H., Lee, D. H., Kung, G. T. C., & Juang, C. H. (2009). Simplified DMT-based methods for evaluating liquefaction resistance of soils. Engineering Geology, 103(1–2), 13–22. https://doi.org/10.1016/j.enggeo.2008.07.008

[40] Robertson, P. (2012). Interpretation of in-situ tests- some insights. 4th International Conference on Site Characterization.

[41] Marchetti, S. (2016). Incorporating the Stress History Parameter KD of DMT into the Liquefaction Correlations in Clean Uncemented Sands. Journal of Geotechnical and Geoenvironmental Engineering, 142(2). https://doi.org/10.1061/(asce)gt.1943-5606.0001380

[42] Chiaradonna, A., & Monaco, P. (2022). Assessment of liquefaction triggering by seismic dilatometer tests: comparison between semi-empirical approchaes and non-linear dynamic analyses. In Rhaman & M. Jaksa (Eds.), Proceedings of the 20th International Conference on Soil Mechanics and Geoetechnical Engineering. Australian Geomechanics Society.

[43] Andrus, R., & Stokoe, K. (2000). Liquefaction Resistance of Soils from Shear-Wave Velocity. Journal of Geotechnical and Geoenvironmental Engineering.

[44] Kayen, R., Moss, R., Thompson, E., Seed, R., Cetin, K., Der Kiureghian, A., Tanaka, Y., & Tokimatsu, K. (2013). Shear-Wave Velocity-Based Probabilistic and Deterministic Assessment of Seismic Soil Liquefaction Potencial. Journal of Geotechnical and Geoenvironmental Engineering, 139.

[45] Marchetti, S., Crapps, D. K. (1981). "Flat Dilatometer Manual", G.P.E. Inc, Italy.

[46] Marchetti, S. (1982). Detection of liquefiable sand layers by means of quasi static penetration tests. 2nd European Symp. on Penetration Testing.

[47] Robertson, P., & Campanella, R. (1986). Estimating liquefaction potential of sands using the plate dilatometer. Geotechnical Testing Jorunal.

[48] Reyna, F., & Chameau, J. (1991). Dilatometer based liquefaction potential of sites in the imperial valley. 2nd International Conference on Recent Advances in Geotechnical.

[49] Yu H. S. (2004). James K. Mitchell Lecture. In situ soil testing: from mechanics to interpretation. In Viana da Fonseca & Paul Mayne (Eds.), Proceedings ISC-2 on Geothecnical and Geophysical Site Characterization.

[50] Amoroso, S., Rollins, K. M., Minarelli, L., Monaco, P., Wissman., K. J. (2024). "Improved Liquefaction Resistance with Rammed Aggregate Piers Resulting from Increased Earth Pressure Coefficient and Density". Journal of Geotechnical and Geoenvironmental Engineering. Vol 150-No. 6. https://doi.org/10.1061/JGGEFK.GTENG-11727

[51] Seed, H., & Idriss, I. (1971). Simplified procedure for evaluating soil liquefaction potential. Journal of Soil Mechanics and Foundation Engineering.

[52] Youd, T., Idriss, I., Andrus, R., Arango, I., Castro, G., Christian, J., Dobry, R., Finn, W., Harder, L., Hynes, M., Ishihara, K., Koester, J., Liao, S., Marcuson, W., Martin, G., Mitchell, J., Moriwaki, Y., Power, M., Robertson, P., … Stokoe, K. (2001). Liquefaction Resistance of soil: summary report from the 1996 NCEER and 1998 NCEER/NSF workshops on evaluation of liquefaction resistance of soils. Journal of Geotechnical and Geoenvironmental Engineering.

[53] Youngs, R. R., Chiou, S.-J., Silva, W. J., & Humphrey, J. R. (1997). Strong Ground Motion Attenuation Relationships for Subduction Zone Earthquakes. Seismological Research Letters, 68(1), 58–73. https://doi.org/10.1785/gssrl.68.1.58

[54] Atkinson, G. M., & Boore, D. M. (2006). Earthquake ground-motion prediction equations for eastern North America. Bulletin of the Seismological Society of America, 96(6), 2181–2205. https://doi.org/10.1785/0120050245

[55] Zhao, J., Zhang, J., Akihiro, A., Ohno, Y., Oouchi, T., Takahashi, T., Hiroshi, O., Irikura, K., Thio, H., Somerville, P., Fukushima, Y., & Fukushima, Y. (2006). Attenuation relations of strong ground motion in Japan using site classification based on predominant period. Bulletin of the Seismological Society of America, 96. https://doi.org/10.1785/0120050122

[56] Iwasaki T., Tokida K., & Arakawa T. (1982). Simplified procedures for assessing soil liquefaction during earthquakes. Proc. Conf. on Soil Dinamycs and Earthquake Engineering, 925–939.

[57] Maurer, B. W., Green, R. A., & Taylor, O. D. S. (2015a). Moving towards an improved index for assessing liquefaction hazard: Lessons from historical data. Soils and Foundations, 55(4), 778–787. https://doi.org/10.1016/j.sandf.2015.06.010

[58] Zhang, G., Robertson, P. K., & Brachman, R. W. I. (2002). Estimating liquefaction-induced ground settlements from CPT for level ground. Canadian Geotechnical Journal, 39(5), 1168–1180. https://doi.org/10.1139/t02-047

[59] Tonkin & Taylor, Ltd, 2013. Liquefaction Vulnerability study, Report to Eaerhquake commission, Tand T ref. 52020.0200/v1.0, prepared by S. van Ballegooy and P. Malan.

[60] Chiaradonna, A., Lirer, S., & Flora, A. (2020). A liquefaction potential integral index based on pore pressure build-up. Engineering Geology, 272. https://doi.org/10.1016/j.enggeo.2020.105620

CERTIFICACIÓN DE REVISIÓN DE PROYECTO DE TITULACIÓN

Por medio de la presente, Yo Davide Besenzon Venegas, Coordinador del Programa de Maestría en Geotecnia de la Escuela Superior Politécnica del Litoral (ESPOL), certifico que:

Con fecha 29 de enero de 2024, el estudiante Christian Marcelo Ramírez Carvajal con número de identificación 0930719596, de la Cohorte 5, presentó la propuesta de su tema de titulación al Comité Académico del programa. Posteriormente, con fecha 31 de mayo de 2024, el Comité revisó y aprobó la propuesta mediante la FICT-CA-GEOTEC-011-2024, cumpliendo con los requisitos establecidos para la aprobación del tema.

A partir de dicha aprobación, el estudiante mantuvo reuniones periódicas con el tutor designado, Davide Besenzon Venegas, para la elaboración y desarrollo de su proyecto de titulación, siguiendo los lineamientos establecidos por el programa. Con fecha 12 de junio de 2024, el estudiante presentó y sustentó su proyecto de titulación ante el tribunal evaluador asignado, cumpliendo con el proceso formal de evaluación académica.

Por lo tanto, en calidad de Coordinador del Programa de Maestría en Geotecnia, certifico que el trabajo de titulación denominado **"Licuación inducida por el terremoto Mw6.6 de Balao en Puerto Baquerizo (Ecuador) y su correlación con la evaluación del potencial de licuación usando SDMT y CPTu"**, realizado el estudiante Christian Marcelo Ramírez Carvajal con número de identificación 0930719596, ha sido revisado y evaluado conforme a los lineamientos y estándares establecidos por el programa.

Debido a circunstancias externas, no ha sido posible obtener las firmas de los involucrados (estudiante, tutor(es) y/o evaluadores). No obstante, en calidad de Coordinador del Programa, certifico que el proyecto cumple con los requisitos académicos y ha sido revisado para su presentación y archivo institucional.

Atentamente,

Firmado electrónicamente por:
ANDRES EDUARDO
GUZMAN VELASQUEZ

M. Sc. Andrés Eduardo Guzmán Velásquez
Coordinador General de Postgrados FICT